Pergamon

Int. J. Heat Mass Transfer. Vol. 37, Suppl. 1, pp. 347–360, 1994

0017–9310/94 $6.00 + 0.00

0017–9310(93)E0056–M

Rationalization of existing mechanistic models for the prediction of water subcooled flow boiling critical heat flux

G. P. CELATA, M. CUMO, A. MARIANI, M. SIMONCINI and G. ZUMMO

ENEA—Energy Department, C.R.E. Casaccia, Via Anguillarese 301, 00060 Rome, Italy

Abstract—This paper presents an analysis of the critical heat flux (CHF) of subcooled flow boiling based on the liquid sublayer dryout mechanism, i.e. the dryout of a thin liquid layer beneath an intermittent vapour blanket due to the coalescence of small bubbles. Starting from the same basic mechanism adopted in earlier models, a new model is derived for the analysis of the CHF in subcooled flow boiling under conditions of very high mass flux and liquid subcooling, typical of fusion reactors thermal hydraulic design. The model is characterized by the absence of empirical constants always present in earlier models. Predicted CHF values are compared with data of 1888 data points for water, showing a good agreement both in precision and in accuracy.

1. INTRODUCTION

THE CRITICAL heat flux (CHF) in water subcooled flow boiling at high mass flux and subcooling has been studied recently in relation with the cooling of high heat flux components in thermonuclear fusion reactors. The above thermal hydraulic conditions, coupled with relatively small tube diameters and lengths, allow us to reach very high values of the CHF, up to some tens of MW m^{-2}. A very recent state-of-the-art review has been proposed by Celata [1].

For calculation and design purposes it is necessary to have reliable predictive tools, such as correlations and models. With regard to correlations, recent papers by Inasaka and Nariai [2], Yin *et al.* [3] and Celata *et al.* [4] showed that few of the existing correlations may provide consistent predictions of water subcooled flow boiling CHF at high heat fluxes. They were originally recommended for operating conditions typical of the Pressurized Water Reactor (i.e. CHF an order of magnitude lower than fusion reactors high heat flux components), in relation to which water subcooled flow boiling CHF was extensively studied in the past [5–6].

As is known, models have the advantage, with respect to correlations, to characterize not only the developing database, but also to be used for the prediction of the CHF beyond the operating conditions of the reference data set. Unfortunately, a full understanding of the basic mechanisms of subcooled flow boiling CHF at high liquid velocity and subcooling has not been accomplished so far [1]. Consequently, existing models [7–9], although mechanistic in nature, make use of empirical correlations or parameters deduced from a best-fit procedure through available data sets. Similarly to correlations, their use outside the experimental ranges of developing data sets cannot therefore be reliable. Even if the Katto model [9] gives an acceptable prediction of existing data points of CHF at high mass flux and subcooling, its use is none the less limited to thermal hydraulic conditions for which high exit bulk subcooled conditions are obtained (i.e. almost 51% of existing data points) [4].

The aim of the present paper is to provide an improvement of existing models, starting from acknowledged basic hypotheses, directly borrowed from existing models [8, 9] and trying to eliminate all the empiricisms through a rationalization process in the description of the dynamics of bubbles in the near-wall region.

2. BACKGROUND

Basic mechanisms of CHF in subcooled flow boiling, usually studied by optical techniques, were outlined by Tong *et al.* [10], Fiori and Bergles [11], Molen and Galjee [12], Hino and Ueda [13] and Mattson *et al.* [14]. The main achievements have already been reported by Weisman and Ileslamlou [7], Lee and Mudawar [8] and Katto [9]. For convenience of the reader they are briefly summarized hereafter: (i) through photography or other means, the existence of vapour slugs or thin vapour layers near the wall was evidenced [10–13]; (ii) wall temperature fluctuations prior to CHF were detected in uniformly heated channels [11]; (iii) no abrupt visible change in the bulk flow pattern at CHF was observed [14]; (iv) the largest bubbles or vapour slugs are generated by the coalescence of smaller bubbles within the two-phase boundary layer in the wall region [12–14]. It has to be pointed out, however, that the basic mechanisms of CHF in subcooled flow boiling at high liquid velocity (up to 40 m s^{-1}) and subcooling (up to 250 K), i.e. including the operating conditions of interest to fusion reactors, are still to be understood, in spite of the many experimental data carried out in the recent past [1]. The great difficulty in applying optical techniques under the above thermal hydraulic conditions, that means fast and very small bubbles (whose diameter is

NOMENCLATURE

C_D drag coefficient [dimensionless]
CHF critical heat flux [W m^{-2}]
C_p specific heat at constant pressure [J kg^{-1} K^{-1}]
D diameter [m]
f friction factor [dimensionless]
$f(\beta)$ function of contact angle, 0.02–0.03 [dimensionless]
G mass flux [kg m^{-2} s^{-1}]
g gravitational acceleration [m s^{-2}]
K thermal conductivity [W m^{-1} K^{-1}]
L length [m]
p pressure [MPa]
Pr Prandtl number, $C_p \mu/K$ [dimensionless]
Q group defined in equation (16)
q'' heat flux [W m^{-2}]
R radius [m]
Re Reynolds number, GD/μ [dimensionless]
S heat transfer surface [m^2]
T temperature [°C]
U velocity [m s^{-1}]
U^+ non-dimensional velocity, defined in equations (8)–(10)
U_τ friction velocity $(\tau_w/\rho_L)^{0.5}$ [m s^{-1}]
y distance from the heated wall [m]
y^* superheated layer [m]
y^+ non-dimensional distance from the heated wall, defined in equations (8) (10).

Greek symbols
β contact angle [deg]
Γ mass flow rate [kg s^{-1}]
δ liquid sublayer initial thickness [m]
ε surface roughness [m]
λ latent heat of vaporization [J kg^{-1}]
μ dynamic viscosity [kg s^{-1} m^{-1}]
ρ density [kg m^{-3}]
σ surface tension [N m^{-1}]
τ passage time of the vapour blanket [s]
τ_w wall shear stress [MPa].

Subscripts
B pertains to the vapour blanket
in inlet
L pertains to the liquid phase
m mean
sub pertains to subcooled conditions
v pertains to the vapour phase
w pertains to the wall.

around some microns or tens of microns), still prevents us from obtaining the necessary information. What remains to be excluded is the hidden existence of an alternative crisis mechanism due to the sudden coalescence of tiny wall bubbles which, still adhering to the wall and beneath the transient vapour slug, thermally isolate the heating wall from the coolant.

Existing models may be classified according to the basic mechanism assumed by the relative authors as the main cause of the CHF occurrence.

(1) Liquid layer superheat limit model. The difficulty of heat transport through the bubbly layer causes a critical superheat in the liquid layer adjacent to the wall, giving rise to the occurrence of the CHF [15].

(2) Boundary layer separation model. This model is based on the assumption that an 'injection' of vapour from the heated wall into the liquid stream causes a reduction of the velocity gradient close to the wall. Once the vapour effusion increases beyond a critical value, the consequent flow stagnation is assumed to originate CHF [16–21]. The weak physical basis of the model has been demonstrated by the studies reported above [11–14].

(3) Liquid flow blockage model. It is assumed that the CHF occurs when the liquid flow normal to the wall is blocked by the vapour flow. Bergel'son [22] considers a critical velocity raised by the instability of the vapour–liquid interface, while Smogalev [23] considers the effect of the kinetic energy of vapour flow overcoming that of the counter motion of liquid.

(4) Vapour removal limit and near-wall bubble crowding model. It is assumed that the turbulent interchange between the bubbly layer and the bulk of the liquid may be the limiting mechanism leading to the CHF occurrence. CHF occurs when bubble crowding near the heated wall prevents the bulk cold liquid from reaching the wall [24]. Weisman and Pei [25], and Weisman and Ying [26] postulate that CHF occurs when the void fraction in the bubbly layer, calculated under the assumption of homogeneous two-phase flow in the bubbly layer in ref. [25] and using the slip model in ref. [26], just exceeds the critical value of 0.82. The void fraction in the bubbly layer is determined through the balance between the outward flow of vapour bubbles and the inward liquid flow at the bubbly layer–bulk liquid flow interface. The Weisman and Ileslamlou model [7] is an improvement of the Weisman and Pei model, for subcooled exit conditions. A research work carried out by Styrikovich *et al.* [27] showed that measured void fraction at CHF ranges from as low as 0.3 to as high as 0.95, making the validity of the near-wall bubble crowding models questionable. In addition, the models are quite empirical in the determination of the turbulent exchange in the bubbly layer. Obviously, it is not excluded that, due to differences in the thermal

hydraulic conditions, different crisis mechanisms may be valid in some ranges of the above conditions.

(5) Liquid sublayer dryout model. The model is based on the dryout of a thin liquid sublayer underneath a vapour blanket or elongated bubble, due to coalescent bubbles, flowing over the wall. This model is supported by more recent experimental studies [12–14, 28–31] in the conditions of our interest.

Lee and Mudawar [8] proposed a mechanistic sublayer dryout model which eliminates the need for much of the empiricism found in the above-described subcooled flow boiling CHF models. Unlike most of them, the CHF analysis proposed by Lee and Mudawar is theoretically based, requiring only three empirical constants. The model closely predicts several well-known CHF databases at high pressure (above 5.0 MPa). None the less, as some assumptions are not valid for low-pressure systems (such as the NET divertor), it is not expected to yield accurate CHF predictions at low pressure [4].

Recently, Katto [9] proposed a model for the prediction of subcooled flow boiling CHF in a very extended range of pressure (0.1–20.0 MPa), employing essentially the same theoretical model constructed by Lee and Mudawar. The main differences are in the calculation of the vapour blanket velocity, obtained by an empirically based relation (as a function of Reynolds number, liquid and vapour density, and void fraction), and in the evaluation of the liquid sublayer thickness, that was indirectly modelled using a correlation for pool boiling [32]. The Katto model, although yielding acceptable predictions of very high heat flux CHF data and points to a wide range of pressure, is not able to calculate the CHF in those cases where the local void fraction in the near-wall bubbly layer is higher than 70%. This is the limit considered by the author for the validity of the assumption of homogeneous flow in the bubbly layer. It happens in all cases where inlet thermal hydraulic conditions are such that the bulk liquid at the exit is slightly subcooled, and was verified for about 51% of high heat flux CHF data collected so far in the literature [4].

Considering that the Lee and Mudawar model cannot be used properly at low pressure, and in view of the above-described limitations of the Katto model, the authors believe it necessary to accomplish a rationalization of the existing liquid sublayer dryout models. They intend to reach a model description of

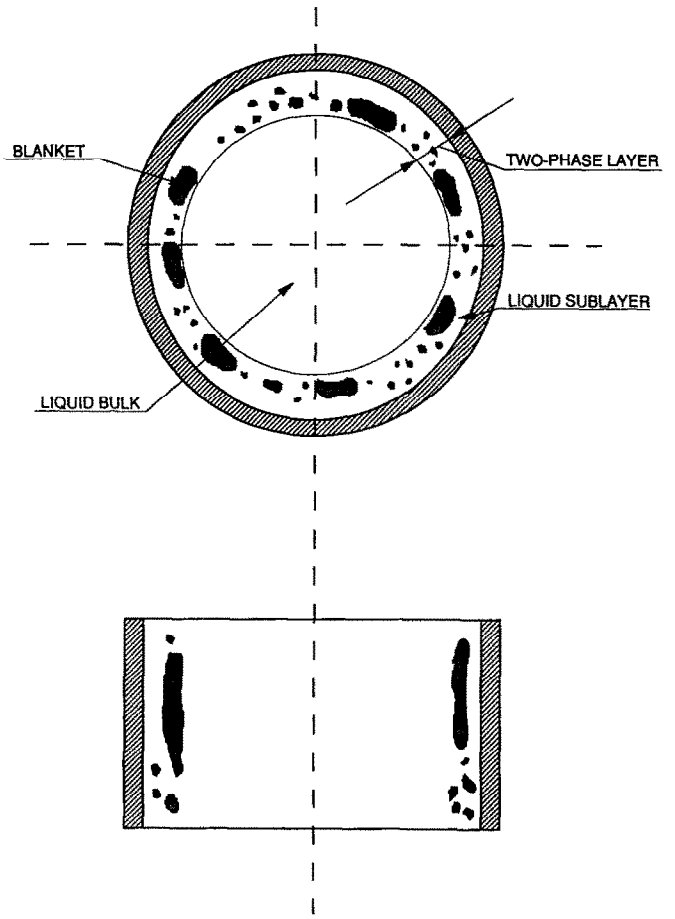

FIG. 1. Schematization of subcooled flow boiling near CHF conditions.

the subcooled flow boiling CHF that, starting from the basic assumptions already proposed by Lee and Mudawar and by Katto, allows a precise and accurate prediction of boiling crisis at high velocity and subcooling, without making use of empirical constants. As already stated above, the basic mechanisms of CHF at high velocity and subcooling are not yet understood. Therefore, the authors wish to call the proposed model a rationalization of those existing, as it is based on the same physical evidences, while proposed modifications are deduced on a rational basis.

3. THE PROPOSED CHF MODEL

The basic assumptions which the proposed model is based on are exactly the same used by Lee and Mudawar [8] and by Katto [9] (liquid sublayer dryout model); also, some of the definitions reported below are borrowed from them. The reference flow configuration is schematically illustrated in Fig. 1. A thin elongated bubble, called 'vapour blanket', is formed as a consequence of coalescence of small bubbles rising along the near-wall region as vertical distorted vapour cylinders. The vapour blanket is overlying a very thin liquid sublayer adjacent to the wall, and CHF is assumed to occur when the liquid sublayer initial thickness, δ, is extinguished by evaporation during the passage time of the vapour blanket, $\tau = L_B/U_B$, where L_B and U_B are the length and velocity of the vapour blanket, respectively.

As assumed by Lee and Mudawar [8], the circumferential growth of a vapour blanket is strongly limited by adjacent blankets. It is therefore reasonable to assume the equivalent diameter of each blanket, D_B (i.e. its thickness) as approximately equal to the diameter of a bubble at the departure from the wall. It is assumed that departing bubbles may coalesce into a distorted blanket that stretches along the fluid flow direction (due to vapour generation by sublayer evaporation) and keeps almost a constant equivalent diameter (thickness). A continuous blanket may be formed along the inner wall of the tube, as a consequence of circumferential blankets merging. Vapour blanket velocity, U_B, is obtained by superimposing the liquid velocity, calculated using the velocity universal profile, and the relative blanket velocity, with respect to the liquid, deduced from a forces balance applied to the blanket (buoyancy and drag) [8].

Vapour blanket length, L_B, is postulated to be equal to the critical Helmholtz wavelength at the liquid–vapour interface [8, 9].

Vapour blanket can develop and exist only in the near-wall region where the local liquid temperature is above the saturation value. Considering the temperature distribution from the heated wall to the centre of the channel, it will exist a distance from the wall at which the temperature, decreasing as we proceed towards the centre of the tube along the radius, is equal to the saturation value at the local pressure. We define this distance as 'superheated layer' and indicate it with y^*, as illustrated in Fig. 2. For a distance from the wall greater than y^*, the blanket (and each single bubble) will collapse in the subcooled liquid bulk. Considering also that the vapour blanket is pushed towards the centre of the tube by the velocity gradient, we assume that the vapour blanket location in the superheated layer is such as to occupy the region closer to the saturation limit, i.e. as far as possible from the heated wall, but within the superheated layer, y^*. The liquid sublayer thickness, δ, can therefore be calculated as the difference between the superheated layer, y^*, and the vapour blanket thickness, D_B.

This basic assumption, based only on a physical consideration, is the main difference between the proposed model and those proposed by Lee and Mudawar and by Katto.

3.1. *Length of vapour blanket*

As discussed above, the liquid sublayer is generally very thin, and it can be roughly assumed to rest on the wall, while the blanket flows at the velocity U_B. It is then postulated that the mean vapour blanket length, L_B, is equal to the critical wavelength of Helmholtz instability of the liquid–vapour interface, and is given by:

$$L_B = \frac{2\pi\sigma(\rho_V + \rho_L)}{\rho_V \rho_L U_B^2}. \tag{1}$$

This is the same procedure and expression used by Lee and Mudawar [8] and by Katto [9].

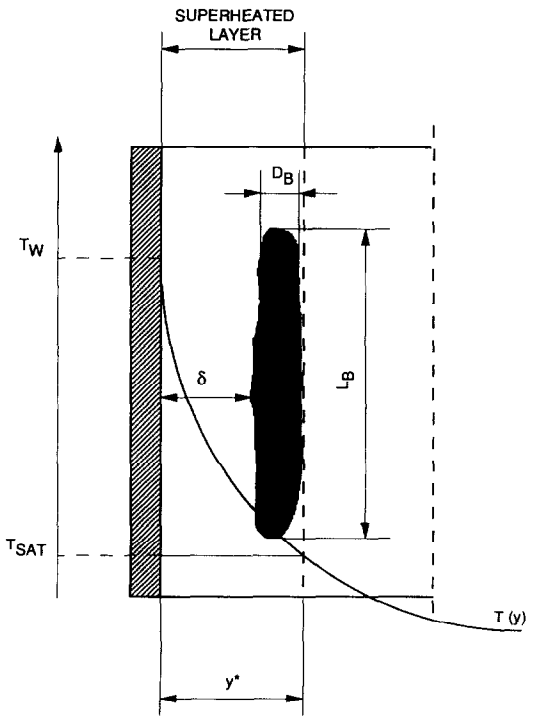

FIG. 2. Schematization of the superheated layer, i.e. the two-phase layer.

3.2. *Velocity of vapour blanket*

As reported by Lee and Mudawar [8], the velocity of the vapour blanket in vertical turbulent flow can be obtained by a forces balance, i.e. buoyancy and drag forces:

$$\frac{\pi}{4} D_B^2 L_B g(\rho_L - \rho_V) = \tfrac{1}{2}\rho_L C_D (U_B - U_{BL})^2 \frac{\pi D_B^2}{4} \quad (2)$$

where C_D is the drag coefficient and $U_B - U_{BL}$ is the relative velocity of the blanket with respect to the liquid at a position corresponding to the centreline of the blanket, given by:

$$U_B - U_{BL} = \left(\frac{2L_B g(\rho_L - \rho_V)}{\rho_L C_D}\right)^{0.5}. \quad (3)$$

The drag coefficient, C_D, is calculated using the equation recommended by Harmathy [33] and Ishii and Zuber [34] for a deformed bubble, the motion of which is determined by buoyancy and surface tension forces, given by:

$$C_D = \frac{2}{3} \frac{D_B}{\left(\dfrac{\sigma}{g(\rho_L - \rho_V)}\right)^{0.5}}. \quad (4)$$

For the evaluation of the vapour blanket equivalent diameter, or thickness, D_B, the model proposed by Staub [35], is used based on a balance of forces to growing bubbles attached to the heated surface, to approximate the diameter of bubbles at departure. In the model, the bubble is considered to detach from the surface when dislodging forces overcome adhesive forces. Among the several forces acting on the bubble (surface tension force, dynamic force due to the momentum change of the liquid resulting from the growing bubble, drag force, buoyancy force, dynamic forces due to the liquid inertia and to the evaporating vapour thrust), Staub considered surface tension force (adhesive) and drag force (dislodging) to be the dominant, and the balance of such forces yields the following expression for D_B

$$D_B = \frac{32}{f} \frac{\sigma f(\beta) \rho_L}{G^2} \quad (5)$$

where β is the contact angle, and $f(\beta)$ is a function that depends only on contact angle. An approximate value for $f(\beta)$ of 0.02–0.03 for water was recommended, and $f(\beta) = 0.03$ is used in the present model.

The friction factor, f, is calculated using the Colebrook–White equation combined with Levy's rough surface model [36], recommended for highly subcooled nucleate boiling. In fact, the pressure drop gradient will increase in the proximity of the CHF, as the bubbles cause an increased surface roughness, but the coolant will still behave as a single-phase fluid. The expression for the friction factor is given by:

$$\frac{1}{\sqrt{f}} = 1.14 - 2.0 \log\left(\frac{\varepsilon}{D} + \frac{9.35}{Re\sqrt{f}}\right) \quad (6)$$

where ε is the surface roughness that has been shown to be close to $0.75 D_B$, D is the inner tube diameter, and Re is the Reynolds number. Considering that $f(\beta) = 0.03$ and $\varepsilon = 0.75 D_B$, the above equation, making use of equation (5), becomes

$$\frac{1}{\sqrt{f}} = 1.14 - 2.0 \log\left(\frac{0.72\sigma\rho_L}{fDG^2} + \frac{9.35}{Re\sqrt{f}}\right). \quad (7)$$

Note the dependence of the friction factor on the surface tension. The solution of this equation for the friction factor requires iteration.

Turning to the calculation of U_B, equation (3), it is now necessary to calculate U_{BL}, i.e. the liquid velocity, U_L, at the centreline of the vapour blanket. The liquid velocity, U_L, for a turbulent flow in a tube as a function of the distance from the wall, y, can be represented by the Karman velocity distribution as

$$U_L^+ = y^+ \quad 0 \leqslant y^+ < 5 \quad (8)$$

$$U_L^+ = 5.0 \ln y^+ - 3.05 \quad 5 \leqslant y^+ < 30 \quad (9)$$

$$U_L^+ = 2.5 \ln y^+ + 5.5 \quad y^+ \geqslant 30 \quad (10)$$

where

$$U_L^+ = \frac{U_L}{U_\tau}, \qquad U_\tau = \left(\frac{\tau_w}{\rho_L}\right)^{0.5},$$

$$y^+ = y \frac{U_\tau}{\mu_L} \rho_L, \quad \tau_w = \frac{fG^2}{8\rho_L}.$$

Calculating U_{BL} as the mean liquid velocity, U_L, at distance $y = \delta + D_B/2$ from the wall using equations (8)–(10), and rearranging equation (3), the vapour blanket velocity, U_B, is given by

$$U_B = \left(\frac{2L_B g(\rho_L - \rho_V)}{\rho_L C_D}\right)^{0.5} + 0.125 f \left(\delta + \frac{D_B}{2}\right) \frac{G^2}{\rho_L \mu_L} \quad (11a)$$

$$U_B = \left(\frac{2L_B g(\rho_L - \rho_V)}{\rho_L C_D}\right)^{0.5} + 1.768\sqrt{f}\frac{G}{\rho_L} \times \left\{\ln\left[0.354 \frac{G}{\mu_L}\sqrt{f}\left(\delta + \frac{D_B}{2}\right)\right] - 0.61\right\} \quad (11b)$$

$$U_B = \left(\frac{2L_B g(\rho_L - \rho_V)}{\rho_L C_D}\right)^{0.5} + 0.884\sqrt{f}\frac{G}{\rho_L} \times \left\{\ln\left[0.354 \frac{G}{\mu_L}\sqrt{f}\left(\delta + \frac{D_B}{2}\right)\right] - 2.2\right\}. \quad (11c)$$

The procedure adopted for the calculation of the vapour blanket velocity is the same as in Lee and Mudawar [8], while the equations used for the evaluation of the blanket equivalent diameter, or thickness, and the friction factor are different. Those used in the

Lee and Mudawar model are not suitable for the operating ranges for which the present model is derived.

3.3. *Initial thickness of liquid sublayer*

As already discussed, the thickness of the liquid sublayer is calculated as the difference between the superheated layer, y^*, and the vapour blanket thickness, or equivalent diameter, D_B

$$\delta = y^* - D_B. \tag{12}$$

As D_B can be calculated by equation (5), it is now necessary to calculate the distance from the wall at which the temperature is equal to the saturation value. The temperature T at a given distance from the wall y, can be obtained using the temperature distribution for turbulent flow in a tube, as proposed by Martinelli [37]

$$T_w - T = Q\,Pr\,y^+ \quad 0 \leqslant y^+ < 5 \tag{13}$$

$$T_w - T = 5Q\left\{Pr + \ln\left[1 + Pr\left(\frac{y^+}{5} - 1\right)\right]\right\} \quad 5 \leqslant y^+ < 30 \tag{14}$$

$$T_w - T = 5Q\left[Pr + \ln(1 + 5Pr) + 0.5\ln\left(\frac{y^+}{30}\right)\right] \quad y^+ \geqslant 30 \tag{15}$$

where T_w is the wall temperature, Pr is the liquid Prandtl number, y^+ is defined above, and Q is a group defined as a function of the local heat flux, q'', the liquid specific heat, C_{pL} and the friction velocity, U_τ

$$Q = \frac{q''}{\rho_L C_{pL} U_\tau}. \tag{16}$$

As the wall temperature T_w is not known (it can only be calculated using empirical correlations), the calculation of the temperature distribution is based on the exit average temperature of the fluid, T_m. This latter is calculated, for a given heat flux q'', by the heat balance in the fluid

$$T_m = T_{in} + \frac{q''\,S}{\Gamma\,C_{pL}} \tag{17}$$

where T_{in} is the liquid inlet temperature, S is the heat transfer surface ($S = \pi D L$), and Γ is the mass flow rate. The average temperature T_m, obtained from equation (17), can be put equal to that calculated using equations (13)–(15)

$$T_m = \frac{5}{y^+(R)}T_{m1} + \frac{25}{y^+(R)}T_{m2} + \frac{y^+(R) - 30}{y^+(R)}T_{m3} \tag{18}$$

being

$$T_{m1} = \frac{1}{5}\int_0^5 T(y^+)\,dy^+ \quad 0 \leqslant y^+ < 5 \tag{19}$$

$$T_{m2} = \frac{1}{25}\int_5^{30} T(y^+)\,dy^+ \quad 5 \leqslant y^+ < 30 \tag{20}$$

$$T_{m3} = \frac{1}{y^+(R) - 30}\int_{30}^{y^+(R)} T(y^+)\,dy^+ \quad y^+ \geqslant 30 \tag{21}$$

and R the radius of the channel. In equation (18), T_w is the only unknown and, therefore, it can be determined. Once T_w is known, it will be possible to calculate the distance from the wall y at which the liquid temperature is equal to the saturation value at the local pressure, i.e. the superheated layer y^*. Now, calculating D_B from equation (5), and from the knowledge of y^*, it is possible to calculate the liquid sublayer thickness δ from equation (12).

This procedure is different from the Lee and Mudawar and Katto models, and allows us to obtain the wall temperature directly from the heat balance, without making use of empirical correlations for the evaluation of the heat transfer coefficient as well as of empirical constants.

3.4. *Critical heat flux*

The critical heat flux, q''_{CHF}, is calculated according to the procedure proposed by Katto [9]. The minimum heat flux necessary to extinguish a liquid sublayer of initial thickness δ by evaporation during the passage time τ of a vapour blanket having a velocity U_B and a length L_B, is

$$q''_{CHF} = \frac{\rho_L\,\delta\,\lambda}{\tau} = \frac{\rho_L\,\delta\,\lambda}{L_B}U_B \tag{22}$$

where ρ_L and λ are the liquid density and the latent heat of vaporization, respectively, both calculated at saturated conditions. Thus, for given geometric and inlet thermal hydraulic conditions, and local pressure p, the critical heat flux q''_{CHF} can be predicted by an iterative procedure through the foregoing equations (1), (4), (5), (7)–(18) and (22).

4. VERIFICATION OF THE CHF MODEL

To verify the accuracy of the proposed model, a CHF database recently gathered by authors under operating ranges typical of fusion reactor thermal hydraulics was used. The data set [39–59] was based on 1888 data points and was detailed in ref. [4], where it was used by the present authors to assess existing correlations and models for the prediction of water subcooled flow boiling CHF at high liquid velocity and subcooling. The database covers the following operating ranges: $0.1 \leqslant p \leqslant 8.4$ MPa; $0.3 \leqslant D \leqslant 25.4$ mm; $0.0025 \leqslant L \leqslant 0.61$ m; $1 \leqslant G \leqslant 90$ Mg m^{-2} s^{-1}; $25 \leqslant \Delta T_{sub,in} \leqslant 255$ K.

Figure 3 shows a comparison of calculated vs experimental CHF, using the above data set. About 91% of data points are predicted within $\pm 30\%$, with a r.m.s. of 17.2%. This is a good performance, also taking into account the wide operating ranges of the

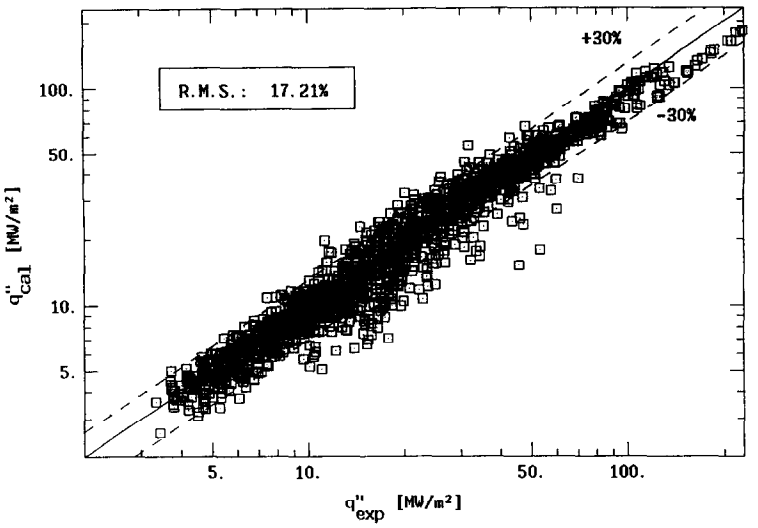

FIG. 3. Calculated vs experimental CHF using the whole data set [39–59].

data set. With reference to the results reported in ref. [4], a comparison between the performances of the Katto model [9] and of the present model has been accomplished. The percentage of data points calculated with a given error band (%) is plotted in Fig. 4 against the error band for the two models. The proposed model provides better predictions than the Katto model all over the error band range, with particular emphasis to the region ± 10–30%. The present model shows also a better global r.m.s. than the Katto model (24.5%). A comparison of the different performance with the single data sets, in terms of r.m.s., is reported in Fig. 5 for the two models.

There is also another significant difference between the two models regarding the number of data points that they are able to predict. While the proposed model is able to calculate all the 1888 data points, the Katto model fails for 961 data points (50.9%). They are discarded because the calculation procedure of the Katto model requires the void fraction in the boiling layer be less than 0.7. This condition is matched whenever the inlet subcooling is medium/low and is associated with low liquid velocity. This is the limit considered by the author for the validity of the assumption of homogeneous flow in the near-wall, two-phase boundary layer. For conditions where a void fraction higher than 0.7 is predicted in the calculation procedure, the model cannot calculate the CHF. Figures 6–10 show the ratio between calculated and experimental CHF vs thermal hydraulic conditions (G, p, x_{ex}) and geometric parameters (L and D), to ascertain possible systematic effects in the model behaviour. A slight underprediction of the CHF can be observed for a mass flux lower than 2 Mg m^{-2} s^{-1}, however, in a region where the CHF is not high (Fig. 6) that is beyond the purposes of the present work. No systematic effect of the pressure is observed (Fig. 7), while a significant underprediction of the CHF is shown for few data points with exit conditions close to saturation (Fig. 8). It is obvious that approaching the saturation conditions, the assumptions made in the construction of the model may not hold any longer, and the model shows a systematic error. Geometric parameters (L/D and D) do not show any systematic influence on the model predictions (Figs. 9 and 10).

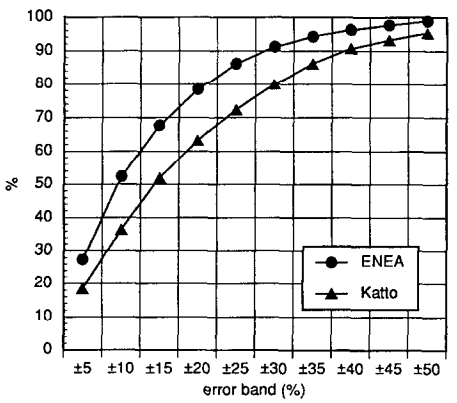

FIG. 4. Percentage of data points predicted within a given error band vs the error band, for the present model and the Katto model [9].

5. PARAMETRIC TRENDS

It is of interest to verify the parametric trends of the model for the subcooled CHF. This latter is a function of thermal hydraulic conditions (mass flux, pressure and subcooling) and geometric parameters (channel diameter and length). The parametric trends of subcooled CHF at medium/low pressure, very high mass flux, high and very high subcooling, and small/very small tube diameter, typical of fusion reactor

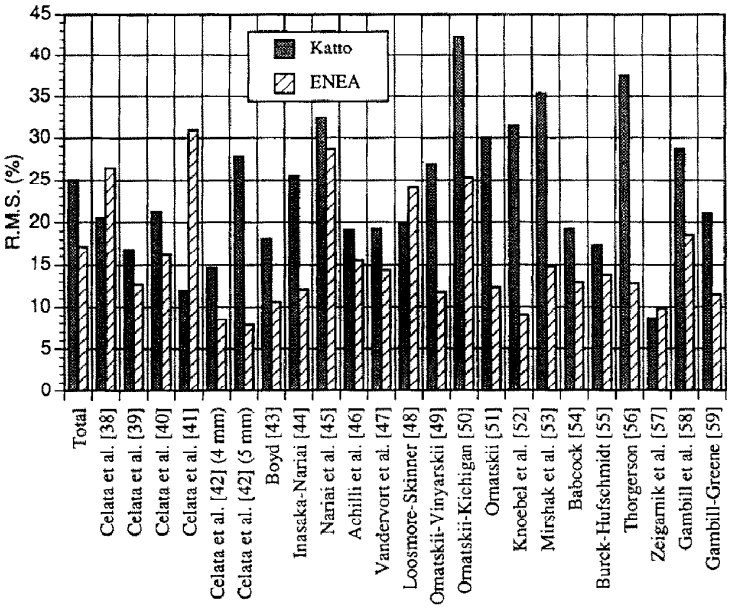

FIG. 5. Calculated r.m.s. errors vs single data sets, for the present model and the Katto model [9].

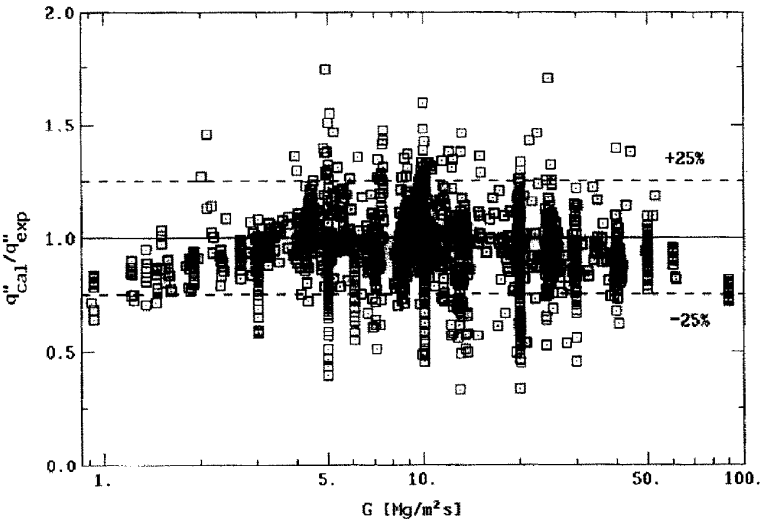

FIG. 6. Ratio of the calculated to the experimental CHF vs mass flux.

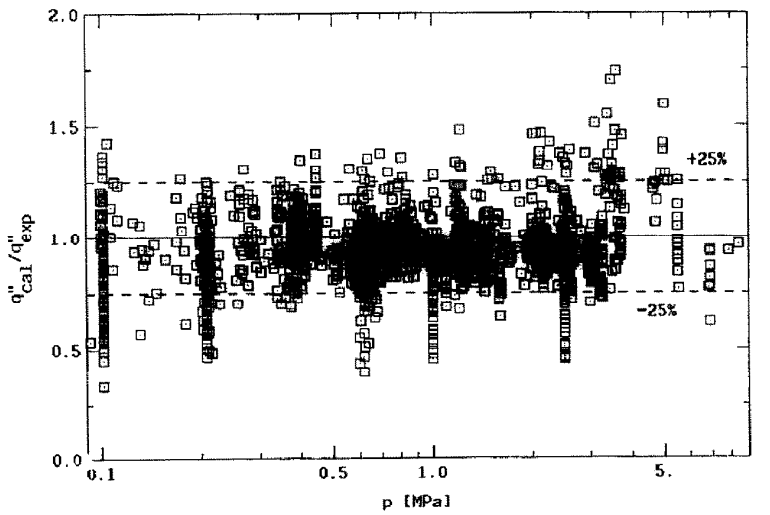

FIG. 7. Ratio of the calculated to the experimental CHF vs pressure.

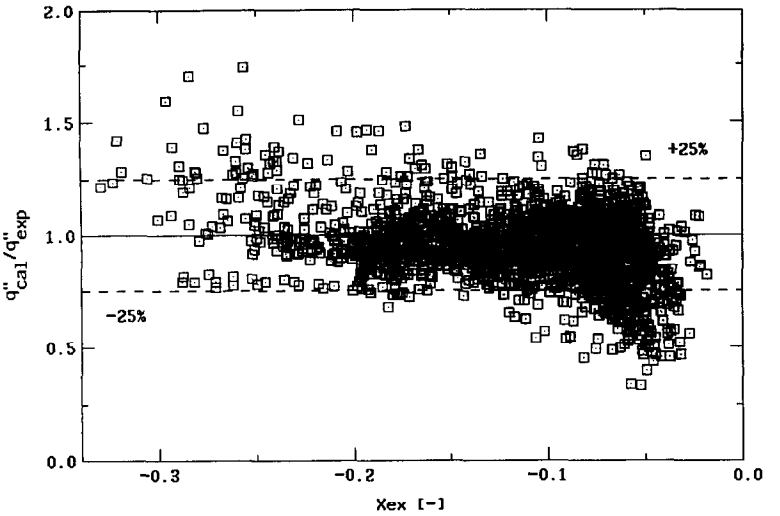

FIG. 8. Ratio of the calculated to the experimental CHF vs exit quality.

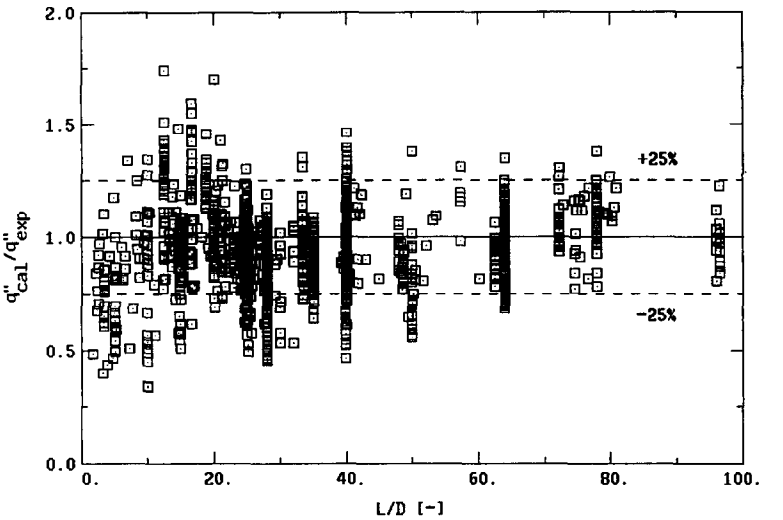

FIG. 9. Ratio of the calculated to the experimental CHF vs L/D ratio.

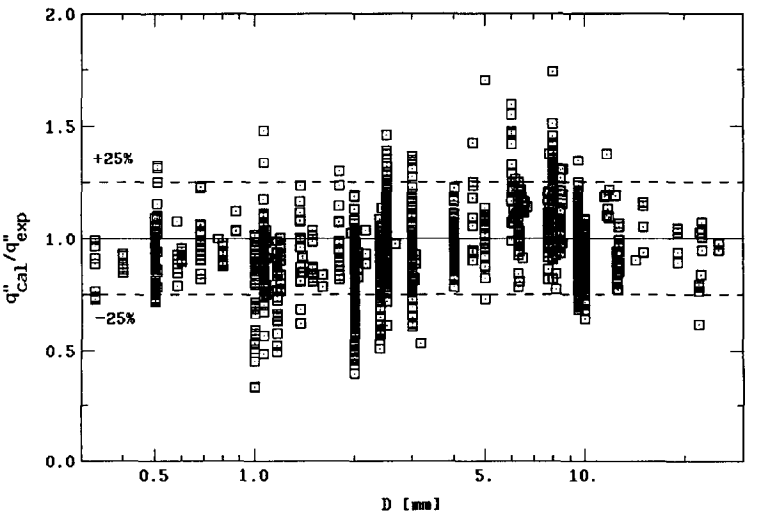

FIG. 10. Ratio of the calculated to the experimental CHF vs channel diameter.

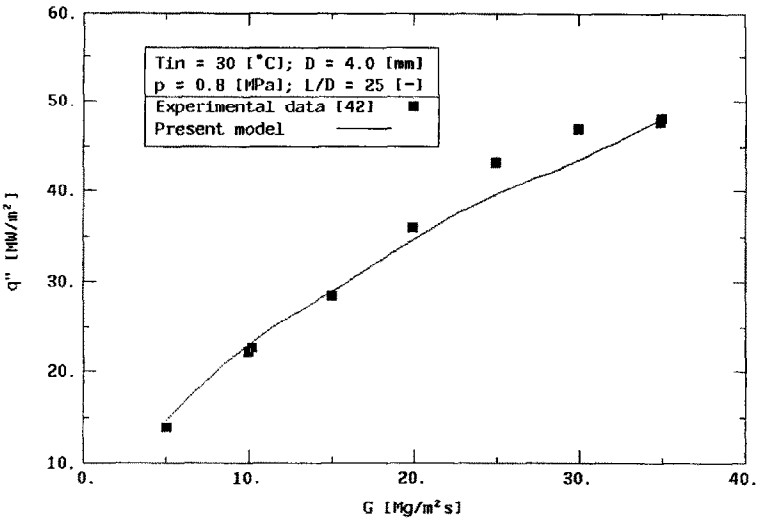

FIG. 11. Mass velocity effect on CHF.

thermal hydraulics, as reviewed by Celata [1], can be summarized as follows.

- CHF increases as mass flux increases.
- CHF is practically independent of pressure.
- CHF increases with increasing degree of subcooling.
- CHF increases as tube diameter decreases.

Figures 11–14 show the calculated and the experimental CHF vs mass flux, pressure, inlet subcooling and exit quality, and tube diameter, respectively, for typical data points selected from the data set. Figure 11 shows that the model provides the same observed experimental trend of CHF vs mass flux, for a wide range of G [42]. The negligible dependence of CHF on exit pressure is matched by the model at low pressure [47] and medium pressure [40], as shown in Fig. 12. The almost linear dependence of the CHF on the liquid subcooling is verified in Fig. 13, where the CHF is plotted vs inlet subcooling [38, 40] (top figure) and exit quality [38, 40, 48, 49, 51] (bottom figure). The dependence of the CHF on D at small diameters is well predicted by the model, together with the interrelation between tube inside diameter and liquid velocity as shown in Fig. 14.

The parametric trends shown in Figs. 11–14, demonstrate that the proposed model is very accurate in predicting independent CHF variations with respect to mass flux, pressure, liquid subcooling and channel diameter.

Finally, to give an idea of the order of magnitude of the several parameters involved in the CHF calculation, Fig. 15 shows the normalized data of the predicted CHF, the vapour blanket velocity U_B, the

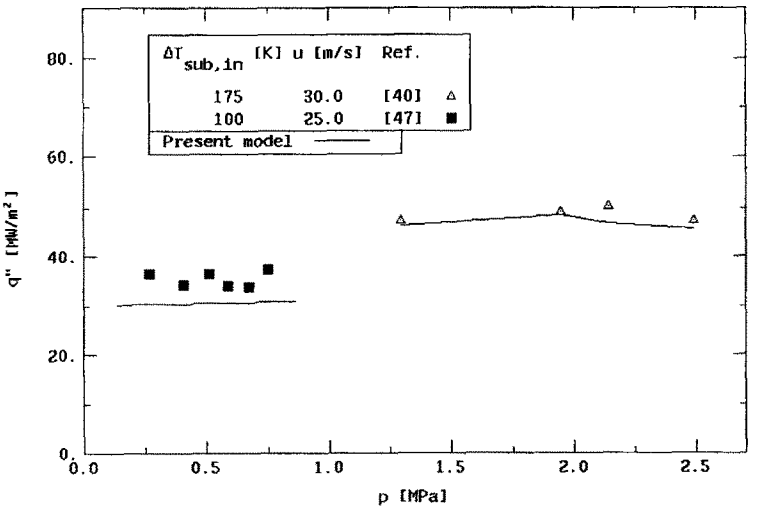

FIG. 12. Pressure effect on CHF.

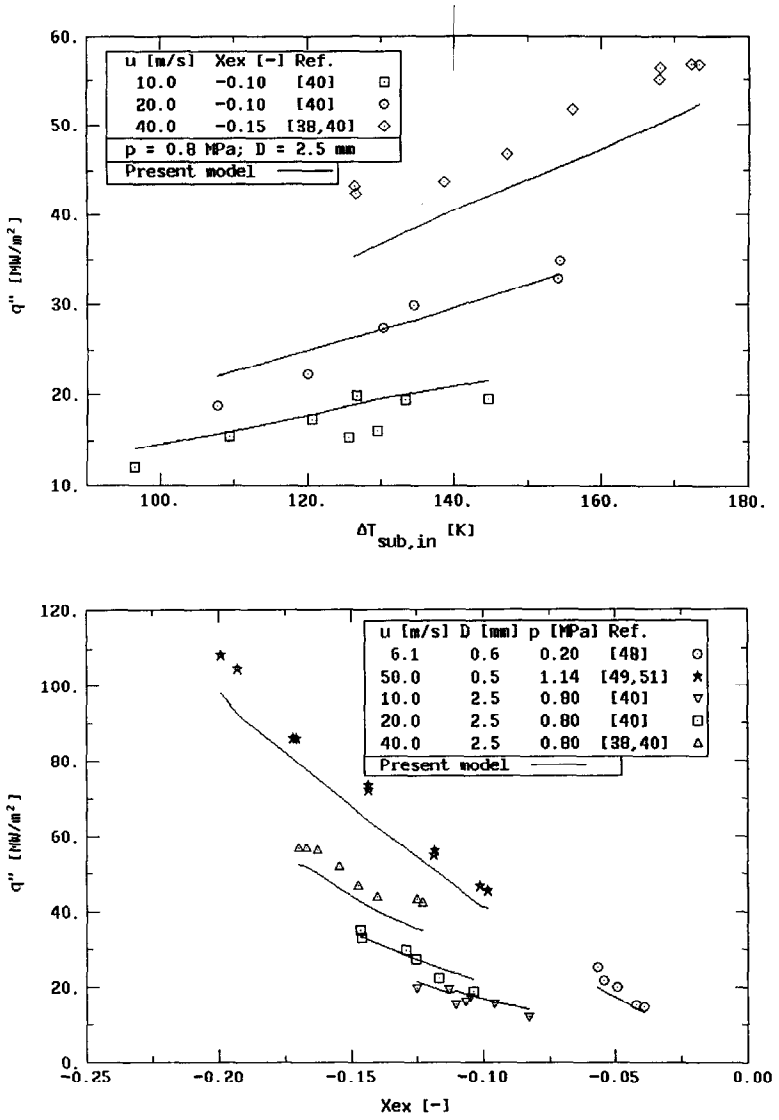

FIG. 13. Inlet subcooling (top figure) and exit quality effect (bottom figure) on CHF.

wall temperature T_w, the initial liquid sublayer thickness δ, the length of the vapour blanket L_B, and its equivalent diameter D_B, as a function of mass flux for data reported in ref. [42] (top figure), and as a function of pressure for data reported in ref. [40] (bottom figure).

6. CONCLUSIONS

A rationalization of existing liquid sublayer dryout models has been accomplished, focusing the proposed new model on physical mechanisms typical of the CHF in subcooled flow boiling at high liquid velocity and subcooling. Similarly to the Lee and Mudawar [8] and Katto [9] models, the proposed model is based on the observation that, during fully developed boiling, a vapour blanket forms in the vicinity of the heated wall by the coalescence of small bubbles, leaving a thin liquid sublayer in contact with the heated wall beneath the blanket. The CHF is assumed to occur when the liquid sublayer is extinguished by evaporation during the passage time of the vapour blanket. The rationalization process allowed us to eliminate any empirical constant present in Lee and Mudawar, and Katto models.

The proposed model has been tested on a wide data set of 1888 data points [39–59], covering the following ranges: $0.1 \leqslant p \leqslant 8.4$ MPa; $0.3 \leqslant D \leqslant 25.4$ mm; $0.0025 \leqslant L \leqslant 0.61$ m; $1 \leqslant G \leqslant 90$ Mg m^{-2} s^{-1}; $25 \leqslant \Delta T_{sub,in} \leqslant 255$ K. The comparison with experimental data showed a good precision, 86% of data points predicted within $\pm 25\%$ (91% within $\pm 30\%$), with a r.m.s. of 17.2%. The analysis of parametric trends demonstrated the good accuracy of the model with regard to variations of mass flux, pressure, subcooling and tube diameter.

The proposed model is particularly useful in the

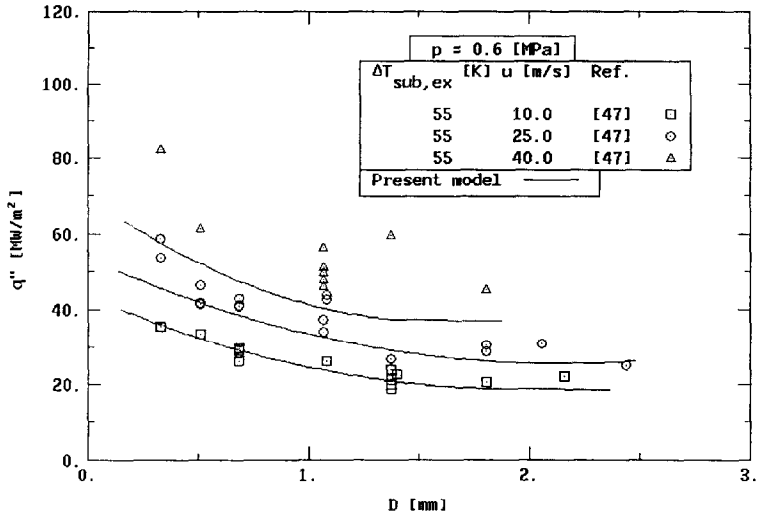

FIG. 14. Diameter effect on CHF.

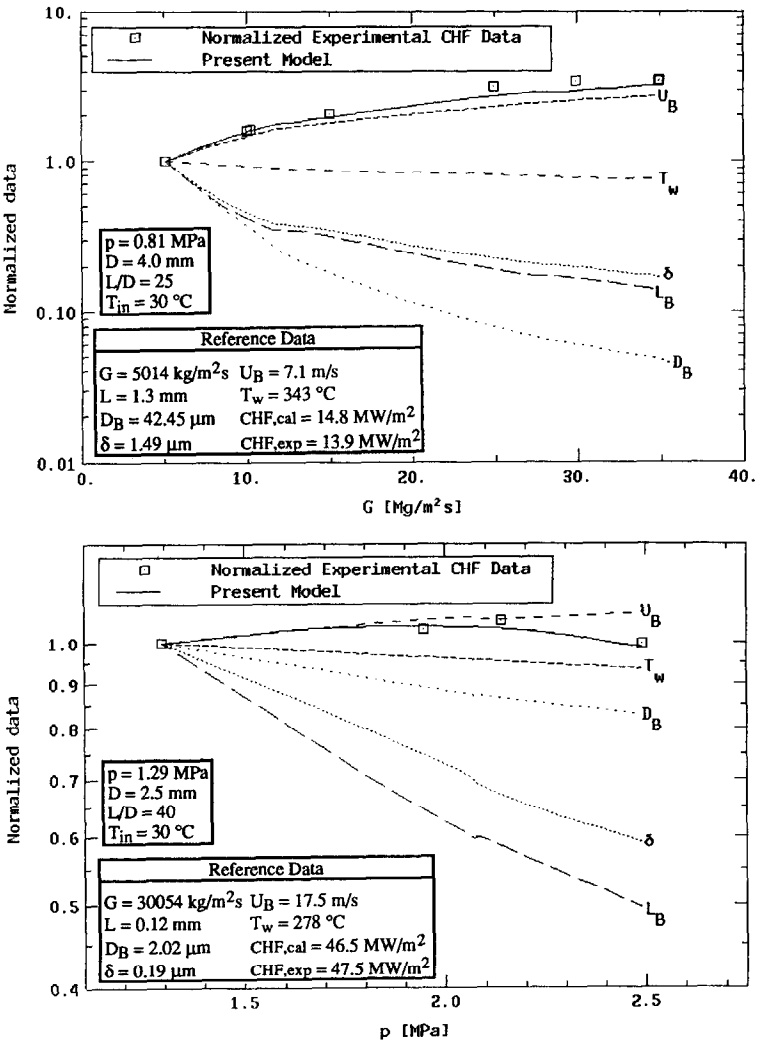

FIG. 15. Typical values of predicted CHF, blanket velocity, wall temperature, initial sublayer thickness, blanket length and equivalent diameter, as a function of mass flux [42] (top figure) and pressure [40] (bottom figure).

thermal hydraulic design of fusion reactor high heat flux components.

Acknowledgement—The authors wish to thank Mrs A. M. Moroni for her precious help in the editing of the paper.

REFERENCES

1. G. P. Celata, Recent achievements in the thermal hydraulics of high heat flux components in fusion reactors, *Expl Thermal Fluid Sci.* **7**, 177–192 (1993).
2. F. Inasaka and H. Nariai, Evaluation of subcooled critical heat flux correlations for tubes with and without internal twisted tapes, *Proc. NURETH-5*, Salt Lake City (1992).
3. S. T. Yin, A Cardella, A. H. Abdelmessih, Z. Jin and B. P. Bromey, Assessment of heat transfer correlations package for water-cooled plasma-facing components in fusion reactors, *Proc. NURETH-5*, Salt Lake City (1992).
4. G. P. Celata, M. Cumo and A. Mariani, Assessment of correlations and models for the prediction of CHF in subcooled flow boiling, *Int. J. Heat Mass Transfer* **37**, 237–255 (1994).
5. J. G. Collier, *Convective Boiling and Condensation* (2nd Edn). McGraw-Hill, London (1980).
6. R. D. Boyd, Subcooled flow boiling critical heat flux (CHF) and its application to fusion energy components. Part I: a review of fundamentals of CHF and related data base, *Fusion Technol.* **7**, 7–30 (1985).
7. J. Weisman and S. Ileslamlou, A phenomenological model for prediction of critical heat flux under highly subcooled conditions, *Fusion Technol.* **13**, 654–659 (1988). (Corrigendum in *Fusion Technol.* **15**, 1463 (1989).)
8. C. H. Lee and I. Mudawar, A mechanistic critical heat flux model for subcooled flow boiling based on local bulk flow conditions, *Int. J. Multiphase Flow* **14**, 711–728 (1988).
9. Y. Katto, A prediction model of subcooled water flow boiling CHF for pressure in the range 0.1–20.0 MPa, *Int. J. Heat Mass Transfer* **35**, 1115–1123 (1992).
10. L. S. Tong, L. E. Effering and A. A. Bishop, A photographic study of subcooled boiling flow and DNB of Freon-113 in a vertical channel, ASME Paper 66WA/HT-39 (1966).
11. M. P. Fiori and A. E. Bergles, Model of critical heat flux in subcooled flow boiling, *Proc. 4th Int. Heat Transfer Conf.*, Vol. VI, p. B6.3. Hemisphere, New York (1970).
12. S. B. van der Molen and F. W. B. M. Galjee, The boiling mechanism during burnout phenomena in subcooled two-phase water flows, *Proc. 6th Int. Heat Transfer Conf.*, Vol. 1, pp. 381–385. Hemisphere, New York (1978).
13. R. Hino and T. Ueda, Studies on heat transfer and flow characteristics in subcooled flow boiling—Part 2. Flow characteristics, *Int. J. Multiphase Flow* **11**, 283–298 (1985).
14. R. J. Mattson, F. G. Hammitt and L. S. Tong, A photographic study of the subcooled flow boiling crisis in Freon-113, ASME Paper 73-HT-39 (1973).
15. L. S. Tong, H. B. Currin, P. S. Larsen and O. G. Smith, Influence of axially nonuniform heat flux on DNB, *Chem. Engng Prog. Symp. Ser.* **62**(64), 35–40 (1965).
16. S. S. Kutateladze and A. I. Leont'ev, Some applications of the asymptotic theory of the turbulent boundary layer, *Proc. 3rd Int. Heat Transfer Conf.*, Vol. III, pp. 1–6. Hemisphere, New York (1966).
17. L. S. Tong, Boundary layer analysis of the flow boiling crisis, *Int. J. Heat Mass Transfer* **11**, 1208–1211 (1968).
18. L. S. Tong, A phenomenological study of critical heat flux, ASME Paper 75-1-1T-68 (1975).
19. J. C. Purcupile and S. W. Gouse, Jr, Reynolds flux model of critical heat flux in subcooled forced convection boiling, ASME Paper 72-HT-4 (1972).
20. W. T. Hancox and W. B. Nicoll, On the dependence of the flow-boiling heat transfer crisis on local near-wall conditions, ASME Paper 73–HT-38 (1973).
21. E. J. Thorgerson, D. H. Knoebel and J. H. Gibbons, A model to predict convective subcooled critical heat flux, *Trans. ASME, Series C, J. Heat Transfer* **96**, 79–82 (1974).
22. B. R. Bergel'son, Burnout under conditions of subcooled boiling and forced convection, *Thermal Engng* **27**(1), 48–50 (1980).
23. I. P. Smogalev, Calculation of critical heat fluxes with flow of subcooled water at low velocity, *Thermal Engng* **28**(4), 208–211 (1981).
24. W. Hebel, W. Detavernier and M. Decreton, A contribution to the hydrodynamics of boiling crisis in a forced flow of water, *Nucl. Engng Des.* **64**, 433–445 (1981).
25. J. Weisman and B. S. Pei, Prediction of critical heat flux in flow boiling at low qualities, *Int. J. Heat Mass Transfer* **26**, 1463–1477 (1983).
26. J. Weisman and S. H. Ying, Theoretically based CHF prediction at low qualities and intermediate flows, *Trans. Am. Nucl. Soc.* **45**, 832–833 (1983).
27. M. A. Styrikovich, E. I. Newstrueva and G. M. Dvorina, The effect of two-phase flow pattern on the nature of heat transfer crisis in boiling, *Proc. 4th Int. Heat Transfer Conf.*, Vol. 9, pp. 360–362. Hemisphere, New York (1970).
28. R. Mesler, A mechanism supported by extensive experimental evidence to explain high heat fluxes observed during nucleate boiling, *A.I.Ch.E. Jl* **22**, 246–252 (1976).
29. A. M. Bhat, R. Prakash and J. S. Saini, Heat transfer in nucleate pool boiling at high heat flux, *Int. J. Heat Mass Transfer* **26**, 833–840 (1983).
30. A. Serizawa, Theoretical prediction of maximum heat flux in power transients, *Int. J. Heat Mass Transfer* **26**, 921–932 (1983).
31. I. A. Mudawar, T. A. Incropera and F. P. Incropera, Boiling heat transfer and critical heat flux in liquid films falling on vertically-mounted heat sources, *Int. J. Heat Mass Transfer* **30**, 2083–2095 (1987).
32. Y. Haramura and Y. Katto, A new hydrodynamic model of critical heat flux, applicable widely to both pool and forced convection boiling on submerged bodies in saturated liquids, *Int. J. Heat Mass Transfer* **26**, 389–399 (1983).
33. T. Z. Harmathy, Velocity of large drops and bubbles in media of infinite and restricted extent, *A.I.Ch.E. Jl* **6**, 281–288 (1960).
34. M. Ishii and N. Zuber, Drag coefficient and relative velocity in bubbly, droplet or particulate flows, *A.I.Ch.E. Jl* **25**, 843–854 (1979).
35. F. W. Staub, The void fraction in subcooled boiling—prediction of the initial point of net vapour generation, *J. Heat Transfer* **90**, 151–157 (1968).
36. S. Levy, Forced convection subcooled boiling—prediction of vapour volumetric fraction, *Int. J. Heat Mass Transfer* **10**, 951–965 (1967).
37. R. C. Martinelli, Heat transfer to molten metals, *Trans. ASME* **69**, 947–951 (1947).
38. G. P. Celata, M. Cumo and A. Mariani, Experimental results on high heat flux burnout in subcooled flow boiling, *Energia Nucleare* **10**(1), 46–57 (1993).
39. G. P. Celata, M. Cumo and A. Mariani, Subcooled water flow boiling CHF with very high heat fluxes, *Revue Générale de Thermique* **362**, 106–114 (1991).
40. G. P. Celata, M. Cumo and A. Mariani, Burnout in highly subcooled flow boiling in small diameter tubes, *Int. J. Heat Mass Transfer* **36**, 1269–1285 (1991).
41. G. P. Celata, M. Cumo and A. Mariani, CHF in highly subcooled flow boiling with and without turbulence pro-

moters, European Two-Phase Flow Group Meeting, Paper C1, Stockholm, 1–3 June (1992).
42. G. P. Celata, M. Cumo and A. Mariani, ENEA Report (not published).
43. R. D. Boyd, Subcooled water flow boiling at 1.66 MPa under uniform high heat flux conditions, *Proceedings of the ASME Winter Annual Meeting, HTD*, Vol. 119, pp. 9–15 (1989).
44. F. Inasaka and H. Nariai, Critical heat flux of subcooled flow boiling with water, *Proceedings of the NURETH-4*, Vol. 1, pp. 115–120 (1989).
45. H. Nariai, F. Inasaka and T. Shimura, Critical heat flux of subcooled flow boiling in narrow tube, *Proceedings of the ASME-JSME Thermal Engineering Joint Conference*, pp. 455–462 (1987).
46. A. Achilli, G. Cattadori and G. P. Gaspari, Subcooled burnout in uniformly and non-uniformly heated tubes, European Two-Phase Flow Group Meeting, Paper C2, Stockholm, 1–3 June (1992).
47. C. L. Vandervoort, A. E. Bergles and M. K. Jensen, The ultimate limits of forced convective subcooled boiling heat transfer, RPI Report HTL-9 (1990).
48. C. S. Loosmore and B. C. Skinner, Subcooled critical heat flux for water in round tube, S.M. Thesis, Massachusetts Institute of Technology, Cambridge, Massachusetts (1965).
49. A. P. Ornatskii and L. S. Vinyarskii, Heat transfer crisis in a forced flow of underheated water in small bore tubes, *Teplofizika Vysokikh Temperatur (High Temp.)* **3**, 444–451 (1964).
50. A. P. Ornatskii and A. M. Kichigan, Critical thermal loads during the boiling of subcooled water in small diameter tubes, *Teploenergetika* **6**, 75–79 (1962).
51. A. P. Ornatskii, The influence of length and tube diameter on critical heat flux for water with forced convection and subcooling, *Teploenergetika* **4**, 67–69 (1960).
52. D. H. Knoebel, S. D. Harris, Jr, B. Crain and R. M. Biderman, Forced-convection subcooled critical heat flux, DP-1306, E. I. Dupont de Nemours and Company (1973).
53. S. Mirshak, W. S. Durant and R. H. Towell, Heat flux at burnout, DP-355, E. I. Dupont de Nemours and Company (1959).
54. D. F. Babcock, Heavy water moderated power reactors, DP-725, E. I. Dupont de Nemours and Company (1962).
55. E. Burck and W. Hufschmidt, EUR-2432 d (in German), EURATOM (1965).
56. E. J. Thorgerson, Hydrodynamic aspect of the critical heat flux in subcooled convection boiling, Ph.D. Thesis, University of South Carolina (1969).
57. Yu. A. Zeigarnik, N. P. Privalov and A. I. Klimov, Critical heat flux with boiling of subcooled water in rectangular channel with one-sided supply of heat, *Thermal Engng* **28**(1), 40–42 (1981).
58. W. R. Gambill, R. D. Bundy and R. W. Wansbrough, Heat transfer, burnout, and pressure drop for water in swirl flow through tubes with internal twisted tapes, *Chem. Engng Prog. Symp. Ser.* **57**(32), 127–132 (1961).
59. W. R. Gambill and N. D. Greene, Boiling burnout with water in vortex flow, *Chem. Engng Prog.* **54**(10), 68–76 (1958).

APPENDIX: CHF CALCULATION PROCEDURE

Input parameters G, p_{ex}, D, L, T_{in}.

Assume a value of q_1. Necessary physical properties are:

$$C_{pL},\ K_L,\ \mu_L,\ \lambda,\ \rho_L,\ \rho_V,\ \sigma.$$

Where not specified, physical properties are calculated at saturated state at p_{ex}.

$$T_{in}+\frac{q''S}{\Gamma C_{pL}}=\frac{5}{y^+(R)}T_{m1}+\frac{25}{y^+(R)}T_{m2}+\frac{y^+(R)-30}{y^+(R)}T_{m3}$$

where C_{pL} is calculated at $(T_m+T_{in})/2$ and T_{m1}, T_{m2} and T_{m3} are calculated from equations (19)–(21) using the temperature distributions:

$$T_w-T=Q\,Pr\,y^+ \quad 0\leqslant y^+<5$$

$$T_w-T=5Q\left\{Pr+\ln\left[1+Pr\left(\frac{y^+}{5}-1\right)\right]\right\} \quad 5\leqslant y^+<30$$

$$T_w-T=5Q\left[Pr+\ln(1+5Pr)+0.5\ln\left(\frac{y^+}{30}\right)\right] \quad y^+\geqslant 30$$

$$Q=\frac{q''}{\rho_L C_{pL} U_\tau}$$

In the above temperature distribution equations, C_{pL} is calculated at saturated conditions at p_{ex}. From the above calculation T_w is obtained. Using the above temperature distribution equations it is possible to calculate y^*, that is the value of the distance from the heated wall, y, at which the fluid temperature is equal to the saturation value at p_{ex}.

Calculation of D_B:

$$D_B=\frac{32}{f}\frac{\sigma f(\beta)\rho_L}{G^2}$$

where $f(\beta)=0.03$ and the friction factor f comes from

$$\frac{1}{\sqrt{f}}=1.14-2.0\log\left(\frac{0.72\sigma\rho_L}{fDG^2}+\frac{9.35}{Re\sqrt{f}}\right).$$

Calculation of δ:

$$\delta=y^*-D_B.$$

Calculation of C_D:

$$C_D=\frac{2}{3}\frac{D_B}{\left(\dfrac{\sigma}{g(\rho_L-\rho_V)}\right)^{0.5}}.$$

Calculation of U_B and L_B (linked with each other):

$$U_B=\left(\frac{2L_B g(\rho_L-\rho_V)}{\rho_L C_D}\right)^{0.5}+0.125f\left(\delta\frac{D_B}{2}\right)\frac{G^2}{\rho_L\mu_L}$$

$$U_B=\left(\frac{2L_B g(\rho_L-\rho_V)}{\rho_L C_D}\right)^{0.5}+1.768\sqrt{f}\frac{G}{\rho_L}\left\{\ln\left[0.354\frac{G}{\mu_L}\sqrt{f}\left(\delta+\frac{D_B}{2}\right)\right]-0.61\right\}$$

$$U_B=\left(\frac{2L_B g(\rho_L-\rho_V)}{\rho_L C_D}\right)^{0.5}+0.884\sqrt{f}\frac{G}{\rho_L}\left\{\ln\left[0.354\frac{G}{\mu_L}\sqrt{f}\left(\delta+\frac{D_B}{2}\right)\right]-2.2\right\}$$

where L_B is given by

$$L_B=\frac{2\pi\sigma(\rho_V+\rho_L)}{\rho_V\rho_L U_B^2}.$$

Calculation of q''_2:

$$q''_{CHF}=\frac{\rho_L\delta\lambda}{L_B}U_B.$$

The condition of critical heat flux, q''_{CHF}, is reached when $q''_1=q''_2$.